

NON-REFLECTING BOUNDARY CONDITIONS ON UNSTRUCTURED GRIDS

Hans-Peter Kersken^{*1}, Christian Frey²

Institute for Propulsion Technology, German Aerospace Center (DLR),
Linder Höhe, 51147 Cologne, Germany

¹ hans-peter.kersken@dlr.de

² christian.frey@dlr.de

Key words: Unstructured grids, Non-reflecting Boundary Conditions

Abstract. Non-reflecting boundary condition at interfaces for flow simulations in turbomachinery using the method laid out by Giles [1] and Saxer [2] require averages or Fourier decomposition of the flow solution using stations of constant radius at the interface. On structured grids the grid generation process can easily enforce grids having element centers with this property while on unstructured grids this is rarely achievable. We describe an approach which works on an auxiliary mesh with a band structure created from the surface mesh at interfaces and study the influence of the prescribed distribution of the bands on the solution. The effectiveness of the approach is demonstrated by applying it to the simulation of a compressor stage and comparing the results with results obtained by using the existing approach for creating bands and a simulation on a structured grid.

1 INTRODUCTION

In simulations of external flows the boundaries of the computational domain can be placed usually far-off the region of interest. In contrast, simulation of internal flows encountered in turbomachinery design often require to place the “far-field” boundaries very close to the region of interest. This makes simulation results of the flow in turbomachinery much more sensitive to the implementation of the numerical treatment of far field boundary condition than in the case of external flows. Accurate non-reflecting boundary conditions have been developed by Giles [1] for the two-dimensional case and extended to the three-dimensional case in [2] in the context of flow simulations in turbomachinery. The latter essentially applied the results for the two-dimensional case on circumferential bands of surface elements at constant radial height. The grid generation process for structured cartesian grids can account for such a band structure easily. In case of unstructured grids it may be difficult to enforce a banded structure of the grid elements on the boundary due to restrictions of the grid generation tool or requirements on the grid elements quality. We describe here an implementation of the one-dimensional flavour of the non-reflecting boundary conditions for steady flows in DLR’s flow solver TRACE [3] on bands created from an auxiliary mesh.

The current implementation of non-reflecting boundary conditions on unstructured grids creates bands by assigning faces at interfaces of the surface mesh with similar radial position to bands. Computational results obtained by applying boundary condition on these bands often

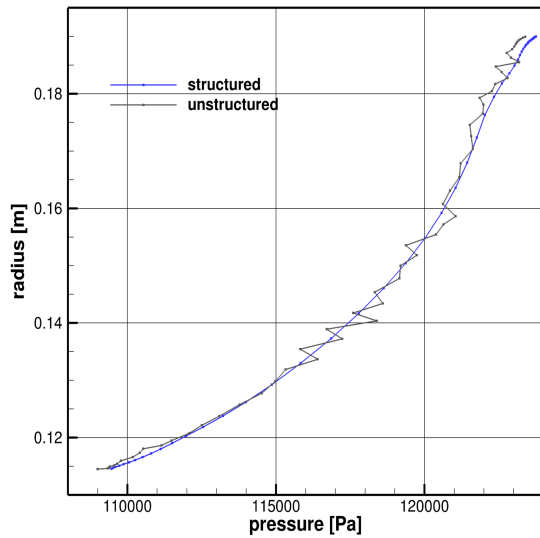


Figure 1: Radial profile of the static pressure at the outlet of a compressor row computed with the unstructured solver with current bands and the structured solver.

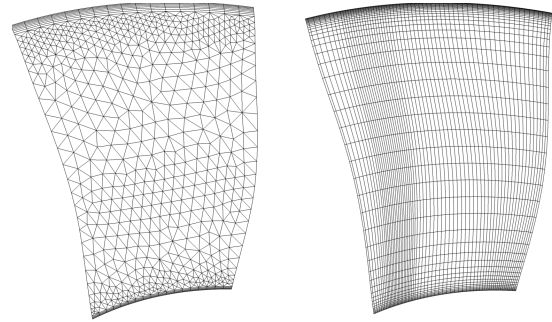


Figure 2: Structured and unstructured grid at the interface used to compute results displayed in Fig. 1.

show erratic changes in, for example, radial profiles of flow variables obtained by circumferential averaging. An example is shown in Fig. 1 and the respective unstructured and structured surface meshes in Fig. 2. To carry over the properties of the non-reflecting boundary conditions on structured grids to unstructured grids independently of the grid generation process we propose to construct an auxiliary grid by prescribing sections bounded by lines of constant radius on the boundary and build an auxiliary grid on these sections based on the original grid. Alternate approaches consist of adding a structured grid section off the interface where boundary conditions are applied or virtual block with the same interface using a chimera like technique to interpolate between the structured and unstructured block. Both have the drawback that additional 3D meshes have to be generated. The option of enforcing a structured surface grid with bands is often ruled out because enforcing it compromises the grid quality in the interior of the domain especially if geometrical details are close to the interface.

2 VIRTUAL BANDS

To construct virtual bands we choose a set of circular arcs at the interface with radii $r_1 < r_2 < r_n$ centered at the intersection of the plane of the interface with the axis of rotation to define the boundaries of the bands. Intersecting these boundaries with the surface grid using the VTK software library [4] yields a new mesh comprising fragments of faces which can uniquely assigned to band. In the following these fragments will be referred to as shards. Figure 3 and Fig. 4 show a section of an unstructured surface mesh cut into shards via this process. Blue dots are used to mark a triangle in the base surface mesh and to highlight its segmentation into shards. These shards are now employed to evaluate the inflow or outflow boundary conditions and for computing circumferential averages.

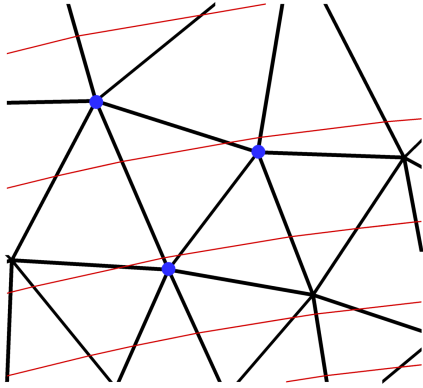


Figure 3: Band boundaries and surface mesh faces.

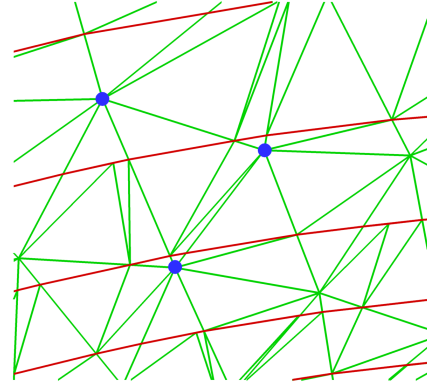


Figure 4: Band boundaries and shards created by intersecting band boundaries with faces.

3 BOUNDARY CONDITION ON VIRTUAL BANDS

The non-reflecting boundary conditions implemented in TRACE use the ideas laid out by Giles for turbomachinery flows, see for example [1] and [2]. Different flavours of this approach has been implemented in TRACE for steady and unsteady flow in the time and frequency domain. They are described in detail for example in [5], [6], and [7]. For the current study we restrict ourselves to the one-dimensional version for steady flows. Figure 5 depicts the overall procedure when the boundary conditions are applied at face (top) and at shards (bottom). The procedure behind the arrow designated by "boundary condition" includes the complete algorithm in [7] for the one-dimensional case of the non-reflecting boundary conditions. Its implementation is

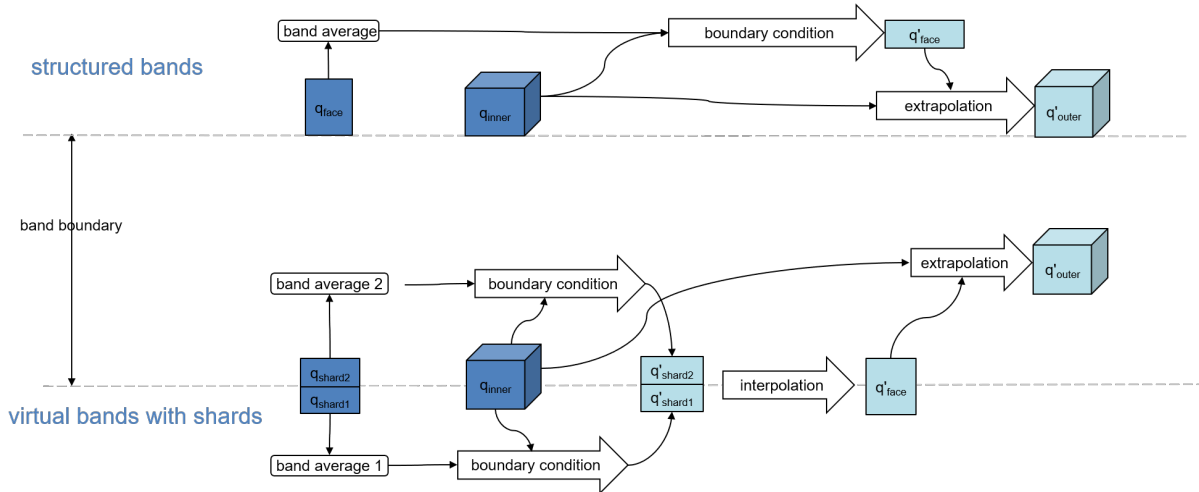


Figure 5: Application of boundary conditions at a regular face not split by a band boundary and a face split into shards by a band boundary.

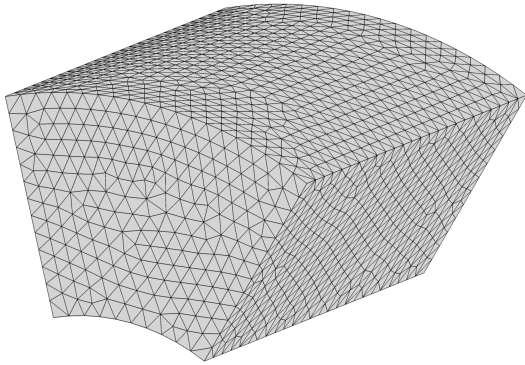


Figure 6: Coarse Mesh for the annular duct.

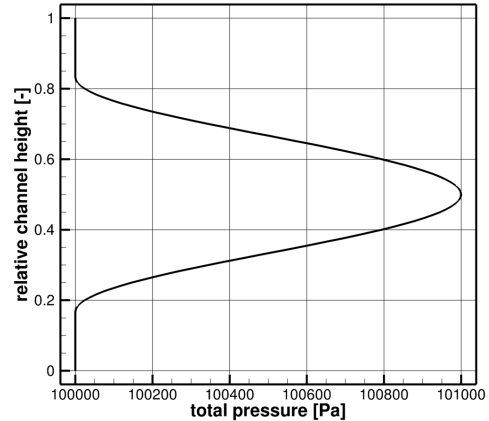


Figure 7: Gaussian-like total pressure profile prescribed at inlet.

identical with the respective version employed at bands created from faces for both the structured and unstructured case. It shows that the procedure is not purely based on interpolation but requires the boundary condition to be applied on the shards. The values at the shards obtained via the application of the boundary are area or flux averaged to its parent face and used to compute circumferential averaged for the band they are assigned to.

4 VERIFICATION AND APPLICATION

We study the accuracy of the obtained solution when virtual bands are employed with respect to the mesh resolution and the number of bands chosen at a duct segment and applied the approach to the simulation of a compressor stage and compare the results on structured and unstructured meshes with and without employing the virtual bands approach.

4.1 Duct segment

For the verification an annular duct segment of length 0.5 m and inner and outer radius of 0.25 m and 0.5 m, respectively, and a circumferential extension of 45° has been used. It has been discretized with three meshes (coarse, medium, fine) comprising approximately 27×10^3 , 0.4×10^6 , and 1.6×10^6 tetrahedral cells. At the boundary at minimal and maximal radius slip boundary condition are applied and periodicity in circumferential direction is assumed. At the inlet and outlet steady one-dimensional boundary conditions on virtual bands are applied. At the inlet a gaussian-like total pressure perturbation in radial direction (see Fig. 7), purely axial flow and a total temperature of 300 K is prescribed. A constant static pressure $p_{out} = 86\,100$ Pa is set at the outlet. The flow is assumed to be inviscid which should result in a constant static pressure of 86 100 Pa throughout the domain for the converged solution. This is what we check for when comparing results at inlet at outlet boundaries. First we compare the accuracy at inlet and outlet for the different mesh resolution. The width of the bands has been chosen to match the average radial extension of the triangles at the surface mesh resulting in 13, 25, and 50 bands

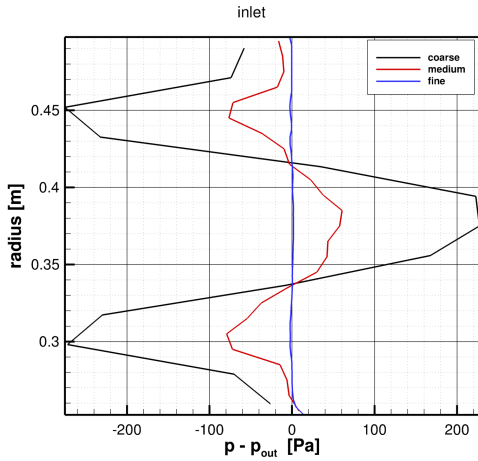


Figure 8: Difference between expected static pressure and simulation result for different mesh resolutions at the inlet.

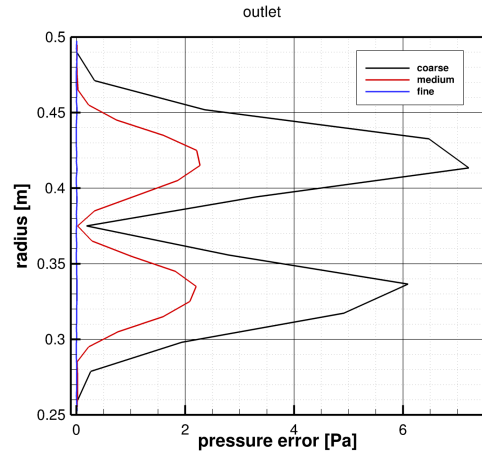


Figure 9: Difference between expected static pressure and simulation result for different mesh resolutions at the outlet.

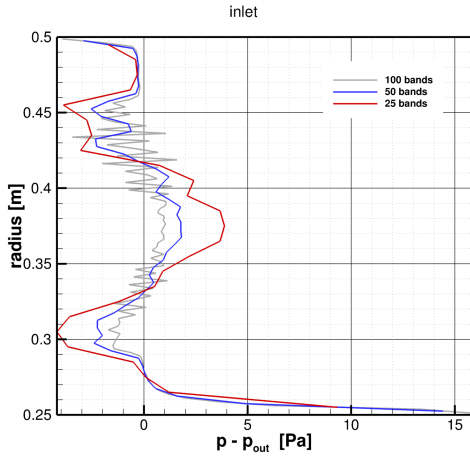


Figure 10: Difference between expected static pressure and simulation result for different number of bands for the fine mesh at the inlet.

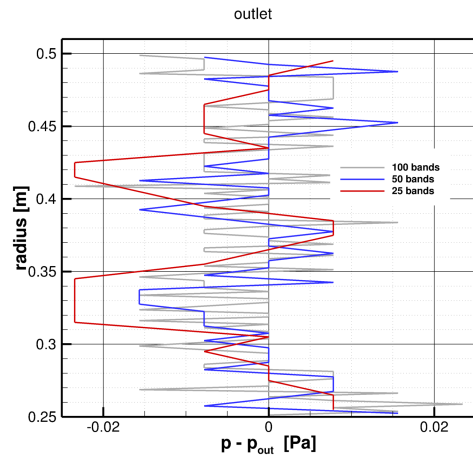


Figure 11: Difference between expected static pressure and simulation result for different number of bands for the fine mesh at the outlet.

for the coarse, medium and fine mesh, respectively. Figure 8 and Fig. 9 display the convergence of the radial pressure distribution to the expected value of 86 100 Pa at the inlet and outlet with increasing mesh resolution. The difference at the outlet is much smaller because we directly prescribe the pressure there while at the inlet it has to be computed from other flow variables. To study further the dependence of the simulation results on the interfaces the number of bands the simulation on the fine grid is repeated with 25 and 100 bands of equal radial height. Again the difference at the outlet is much smaller than at the inlet and almost constant independent of the number of bands as shown in Fig. 11. At the inlet decreasing the number of bands from

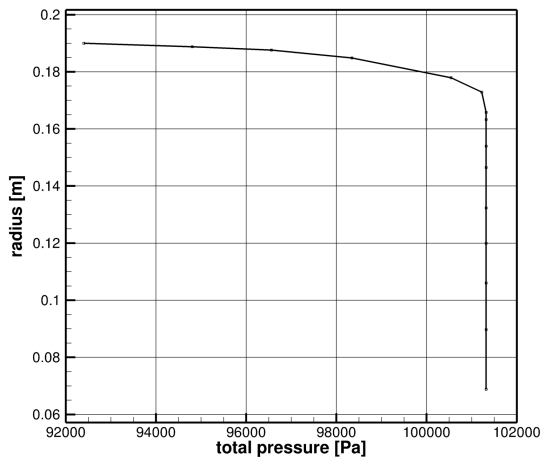


Figure 12: Prescribed total pressure radial profile at the inlet of the compressor stage.

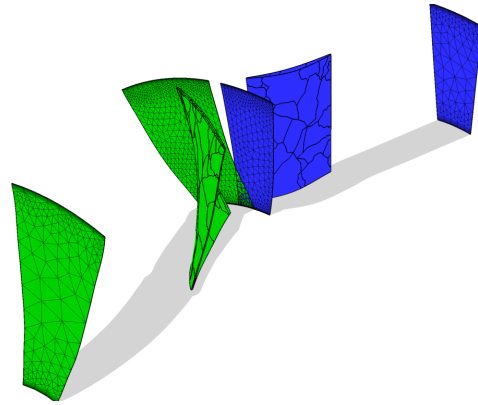


Figure 13: Interfaces and blades of the compressor stage.

50 to 25 lead to a larger difference to the reference profile, i.e. a larger error, while increasing the number of bands to 100 leads to no significant reduction of the difference but to a profile exhibiting large variations (see Fig. 10). Here the spatial resolution of the bands is higher than the resolution of the grid leading inconsistencies when prescribing the total pressure distribution which does not occur at the outlet because the prescribed static pressure does not depend on the radial position. This reveals that the usefulness of the virtual band approach depends strongly on an appropriate choice of the position of the band boundaries.

4.2 Compressor stage

The flow in a single passage of a compressor stage comprising a rotor with 16 and a stator with 29 blades is simulated. The unstructured mesh consists of approximately 6×10^5 tetrahedral and prismatic cells. At the stage inlet the radial distribution of the total pressure profile shown in Fig. 12, purely axial flow and a total temperature of 288.25 K is prescribed. The outlet a static pressure is set to 129 000 Pa and radial equilibrium is enforced. At the interface between the two blade rows we use the mixing plane approach and at all interface we employ the one-dimensional non-reflecting boundary conditions on virtual bands. At walls no-slip boundary conditions are used via the wall function approach. The turbulence is modelled via the $k-\omega$ turbulence model [8].

Additionally, a simulation on a structured grid consisting of approximately 4×10^5 hexahedral cells and a simulation on the unstructured grid but employing bands constructed from faces instead of virtual bands.

While a reasonable band distribution could be defined ad hoc in the case of the duct example here we are faced with widely varying cell sizes at similar radial positions. A priori it is not clear where to place the band boundaries in this case. As a starting point we chose a band distribution derived from the bands created by the approach of grouping faces to bands. For these an average band radius defining the center of the bands can be derived. The band boundaries of the virtual bands are then placed at the average of two adjacent radii. Figure 14 shows the surface mesh

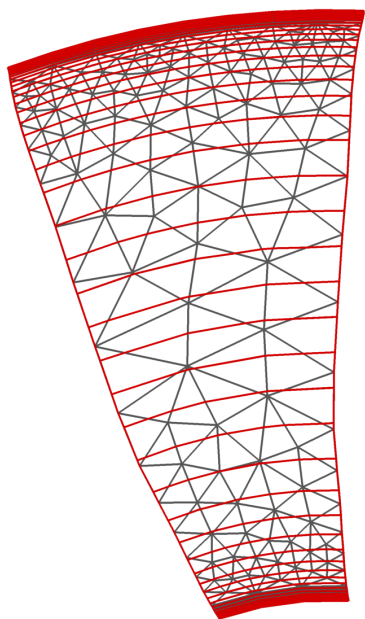


Figure 14: Mesh and band boundaries at the entry of the stage.

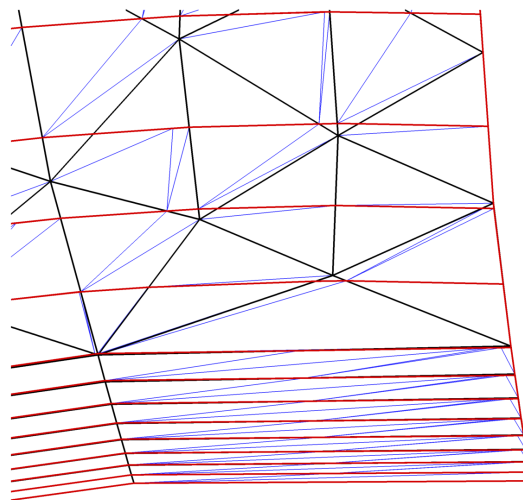


Figure 15: Mesh detail near the hub at the entry of the stage. Band boundaries are colored in red, face edges in black and shad edges in blue.

and the band boundaries at the entry of the stage. As shown in Fig. 15 the method of defining virtual bands by arcs of constant radius may not honor an already existing band structure created by prism layers at surfaces because the vertices of the elements comprising the natural bands may not be placed exactly at the same radius. However, the virtual bands created there are a very good approximation to these naturally available bands. Figure 16 to Fig. 18 show the simulation result for the three different simulations. The results of two simulation on the unstructured grid show an overall good agreement with the result of the simulation on the structured grid (note the different scales for the pressure in the plots). However, the results obtained with the virtual bands approach show a much smoother radial profile at all interfaces than those obtained with the bands from faces approach. In the region close to the boundary layer at the upper wall the result can be improved by manually adapting the band boundaries to the radial height of the triangles. Figure 19 shows exemplarily a section of the mesh at the outlet of the first row including the band boundaries. The adapted band distribution is created by removing the boundaries colored in red. The radial pressure profile in the modified radial region obtained with the adapted band distribution is shown in Fig. 20.

—•— **structured**
—•— **virtual bands**
—•— **bands from faces**

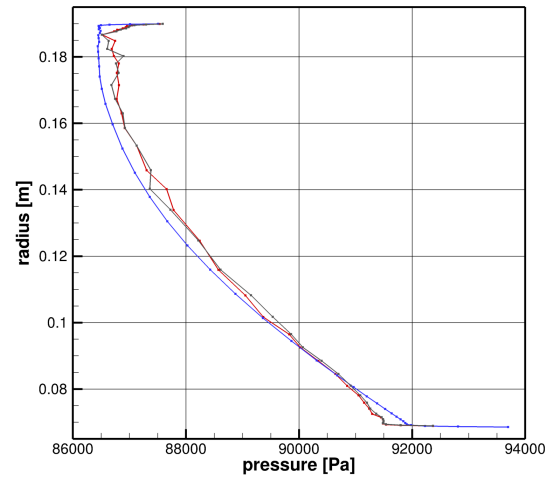


Figure 16: Radial distribution of the static pressure at the stage inlet.

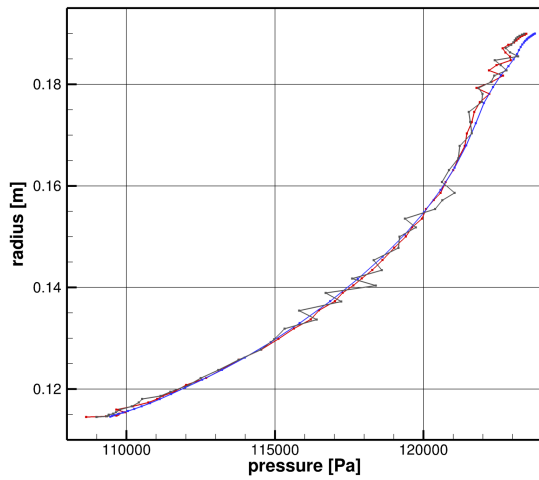


Figure 17: Radial distribution of the static pressure at the outlet of the first row.

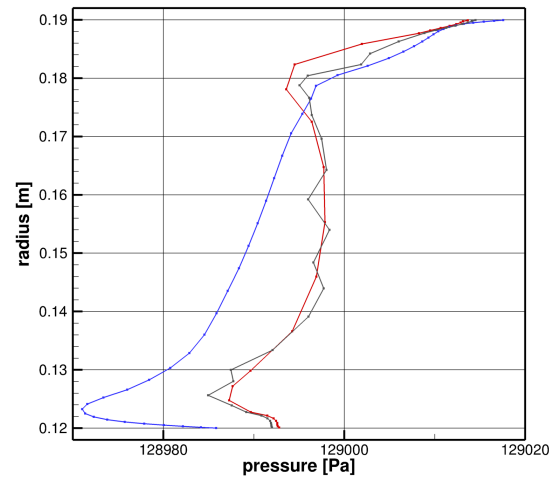


Figure 18: Radial distribution of the static pressure at the stage outlet.

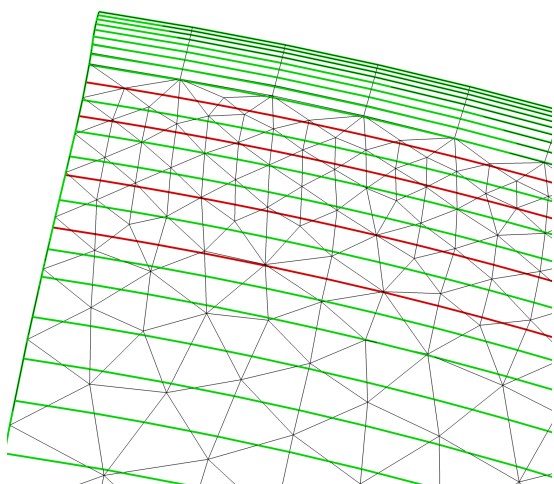


Figure 19: Section of the mesh of the outlet of the first row including the virtual band boundaries.

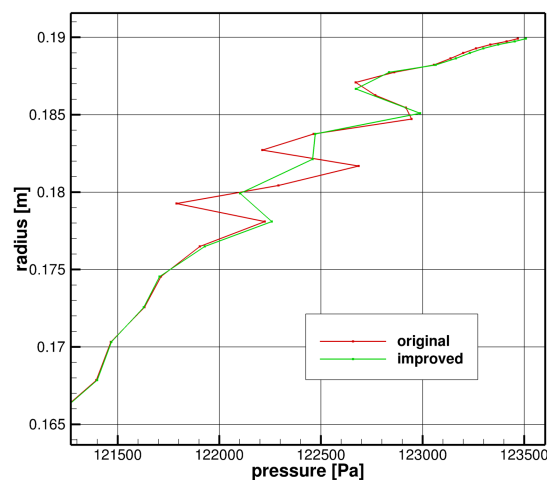


Figure 20: Radial distribution of the static pressure in the region of adapted band distribution.

5 Summary

We described an approach for implementing non-reflecting boundary conditions on unstructured meshes lacking an obvious band structure. A virtual band structure is introduced by defining radial positions of band boundaries at interfaces and creating an auxiliary mesh by intersecting the surface mesh of the 3D mesh with these bands. Circumferential averaging and application of boundary condition employs the faces of the auxiliary mesh. The approach has been applied to the simulation of a transonic compressor stage using the one-dimensional version of the non-reflecting boundary condition at all interfaces. It has been shown that the new approach removes the erratic fluctuation observed with the old approach of grouping faces into bands, but it has been observed that the quality of the solution depends strongly on the band distribution. Further studies are necessary to develop a robust method for determining a band distribution appropriate for arbitrary surface element distributions.

6 Acknowledgements

This research was supported by the German Federal Ministry of Economics and Technology under grant number 20T1719B.

REFERENCES

- [1] M. B. Giles. Nonreflecting boundary conditions for Euler calculations. *AIAA J.*, 28(12):2050–2058, 1990.
- [2] A. P. Saxer and M. B. Giles. Quasi-three-dimensional nonreflecting boundary conditions for Euler equations calculations. *J. Propul. Power*, 9(2):263–271, 1993.
- [3] Kai Becker, Kathrin Heitkamp, and Edmund Kügeler. Recent progress in a hybrid-grid CFD solver for turbomachinery flows. In *Proceedings Fifth European Conference on Computational*

Fluid Dynamics ECCOMAS CFD 2010, Lisbon, Portugal, June 2010.

- [4] W. Schroeder, K. Martin, K.W. Martin, and B. Lorenzen. *The visualization toolkit*. Prentice Hall PTR, 1998.
- [5] D Schlüß, C Frey, and G Ashcroft. Consistent non-reflecting boundary conditions for both steady and unsteady flow simulations in turbomachinery applications. In *ECCOMAS Congress 2016 VII European Congress on Computational Methods in Applied Sciences and Engineering, Crete Island, Greece*, 2016.
- [6] Hans-Peter Kersken, Graham Ashcroft, Christian Frey, Nina Wolfrum, and Detlef Korte. Nonreflecting boundary conditions for aeroelastic analysis in time and frequency domain 3D RANS solvers. In *Proceedings of ASME Turbo Expo 2014*, 2014.
- [7] Sebastian Robens, Christian Frey, Peter Jeschke, Edmund Kügeler, Arianna Bosco, and Thomas Breuer. Adaption of Giles non-local non-reflecting boundary conditions for a cell-centered solver for turbomachinery applications. In *Proceedings of ASME Turbo Expo 2013*, 2013.
- [8] D. C. Wilcox. *Turbulence Modeling for CFD*. DCW Industries, La Cañada, USA, 3 edition, 2006.